THE JOURNAL OF BIOLOGICAL CHEMISTRY VOL. 290, NO. 18, pp. 11491–11503, May 1, 2015


# Wild-type Human γD-crystallin Promotes Aggregation of Its Oxidation-mimicking, Misfolding-prone W42Q Mutant*

Received for publication, October 27, 2014, and in revised form, March 11, 2015 Published, JBC Papers in Press, March 18, 2015, DOI 10.1074/jbc.M114.621581

**Eugene Serebryany and Jonathan A. King**[1]

*From the Department of Biology, Massachusetts Institute of Technology, Cambridge, Massachusetts 02139*

**Background:** Oxidative damage and destabilizing mutations in γ-crystallins lead to cataract disease.
**Results:** Addition of wild-type γD-crystallin promotes aggregation of the oxidation-mimicking W42Q mutant, yet the wild-type protein escapes coaggregation.
**Conclusion:** Wild-type human γD-crystallin can serve as a catalyst for aggregation of its misfolding-prone point mutant.
**Significance:** This finding provides a model of pathology caused by wild-type/mutant or undamaged/damaged protein interactions.

**Non-native protein conformers generated by mutation or chemical damage template aggregation of wild-type, undamaged polypeptides in diseases ranging from amyotrophic lateral sclerosis to cancer. We tested for such interactions in the natively monomeric human eye lens protein γD-crystallin, whose aggregation leads to cataract disease. The oxidation-mimicking W42Q mutant of γD-crystallin formed non-native polymers starting from a native-like state under physiological conditions. Aggregation occurred in the temperature range 35–45 °C, in which the mutant protein began to lose the native conformation of its N-terminal domain. Surprisingly, wild-type γD-crystallin promoted W42Q polymerization in a catalytic manner, even at mutant concentrations too low for homogeneous nucleation to occur. The presence of wild-type protein also downshifted the temperature range of W42Q aggregation. W42Q aggregation required formation of a non-native intramolecular disulfide bond but not intermolecular cross-linking. Transient WT/W42Q binding may catalyze this oxidative misfolding event in the mutant. That a more stable variant in a mixture can specifically promote aggregation of a less stable one rationalizes how extensive aggregation of rare damaged polypeptides can occur during the course of aging.**

Polymerization of partially unfolded protein intermediates occurs in diverse age-related conformational diseases, including amyotrophic lateral sclerosis (superoxide dismutase 1), Parkinson's disease (α-synuclein), serpinopathies ($\alpha_1$-antitrypsin), and many types of cancer (p53) (1–4). Three classes of structured polymers are known (Fig. 1), although in many cases polymers are classified as amorphous for lack of structural data (5). Runaway domain swapping, in which monomers briefly open up or unfold and then exchange identical structural elements to reconstitute the native protein conformation in *trans*, has been found or proposed in a number of such cases (6). Polymerogenic partially unfolded intermediates can be generated by mutations or by post-translational modifications, which often have similar effects (2, 7–10).

The human eye lens is a particularly striking case of protein aging. Fiber cells of the lens core terminally differentiate *in utero*, losing all organelles, as well as protein synthesis and degradation machinery, and are never replaced (11). Crystallins make up >90% of the total protein in this tissue (~400 mg/ml), whose transparency depends on their structural integrity and lack of long range packing (12). Only passive chaperone capacity is present, and it decreases with age, even as destabilizing chemical modifications, such as oxidation, accrue (13). The result is progressive increase in light scattering (lens turbidity) caused by aggregation; this is the basis of cataract disease, a major cause of blindness worldwide (12, 13). No long range structure has been found in the cataractous aggregates (14), but disulfides and other covalent modifications are common (15, 16). Reducing capacity of the lens core cytosol is lost during cataractogenesis (17).

Roughly 20% of total lens protein are the natively monomeric γ-crystallins; the most stable, γD-crystallin (HγD),[2] constitutes 10–20% of those, with higher proportions in the dense lens core (18, 19). The β-sheet rich HγD monomer has a melting temperature of 82 °C and aggregates only under nonphysiological conditions (20). More than 20 point mutations in conserved γ-crystallin residues, particularly near the N-terminal β-strands, are linked to congenital cataract (14). Such mutations can generate conformational intermediates leading to aggregation (8, 21–23). The hydrophobic core of each double-Greek key domain of HγD includes two highly conserved Trp residues (Fig. 2*A*) (24), which can be oxidized to more hydrophilic products upon exposure to UV-B light, opening up the HγD fold (25, 26). We mimicked this type of damage with the W42Q substitution. The W42R mutation was recently reported to cause hereditary cataract (27), suggesting a mechanistic convergence

* This work was supported, in whole or in part, by National Institutes of Health Grant EY015834 from the National Eye Institute (to J. A. K.). This work was also supported by Massachusetts Institute of Technology Biology/Merck academic support fellowships to (E. S.).
[1] To whom correspondence should be addressed: Dept. of Biology, Massachusetts Institute of Technology, 77 Massachusetts Ave. 68–318, Cambridge, MA 02139. Tel.: 617-253-4700; Fax: 617-252-1843; E-mail: jaking@mit.edu.

[2] The abbreviations used are: HγD, human γD-crystallin; TCEP, tris-(2-carboxyethyl) phosphine hydrochloride; bis-ANS, 4,4′-dianilino-1,1′-binaphthyl-5,5′-disulfonic acid; N-td, N-terminal domain; C-td, C-terminal domain.

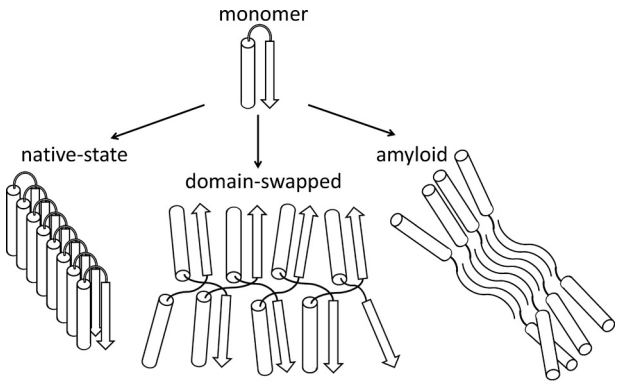


FIGURE 1. **Cartoon representation of the three known classes of structured protein polymers.**

between genetic and sporadic forms of cataract disease. We found that the W42Q mutant is monomeric and folded in storage, but at high concentrations at 37 °C it forms aggregates morphologically similar to those previously obtained by UV-B irradiation (28).

Most conformational disease is sporadic; it is often unclear how homogeneous nucleation of aggregates can occur, because no germ line mutation and only low levels of side chain modifications are present (4). However, deleterious interactions between wild-type and mutant or damaged proteins have recently been reported in diverse cases, from ALS to tumorigenesis (29–31). We tested for such interactions in mixtures of W42Q and wild-type HγD. The mixtures indeed produced much higher light scattering (turbidity) than the mutant protein by itself. Surprisingly, however, the aggregated fraction contained only the mutant, whereas the wild-type HγD escaped coaggregation.

Until now, the templating (prion-like) model has been the only paradigm for non-native polymerization caused by interaction of natively folded proteins with variants prone to misfolding. By contrast, in our mixtures only the mutant aggregates, yet the amplitude, kinetics, and nucleating concentration of the aggregation reaction depend on the sequences of both the aggregating and the nonaggregating constructs. At low mutant concentrations nucleation occurs only in the presence of excess wild-type protein. The properties of W42Q aggregates resemble runaway domain swapping. We propose that a transient mutant/wild-typebindinginteractionspecificallypromotespolymerization of the mutant, whereas the wild type escapes coaggregation and regenerates to a soluble state. We also show that aggregation requires formation of an intramolecular disulfide bond; W42Q molecules that did not form this bond remained soluble.

## EXPERIMENTAL PROCEDURES

*Protein Expression and Purification*—$His_6$-tagged constructs were expressed using the pQE1 plasmid (Qiagen) in M15 *Escherichia coli*. The N-terminal tag sequence was MKHHHHHHQ, as used previously (20). $His_6$-tagged constructs were purified using $Co^{2+}$-NTA columns (Thermo-Fisher) following the manufacturer's instructions. Sample purity was >95% by SDS-PAGE of peak fractions. Three steps of dialysis of at least 4 h each were carried out, one of them against buffer containing 0.1 mM EDTA to remove any residual metal ions. Untagged constructs were expressed using the pET16b plasmid (Novagen) in BL21-RIL *E. coli*. Following transformation cells were grown at 37 °C to $A_{600}$ of ~5 and induced with 1 mM isopropyl β-D-thiogalactopyranoside overnight at 18 °C. Cell pellets were resuspended with lysis buffer (50 mM sodium phosphate, 0.3 M NaCl, pH 7.4) with EDTA-free Complete-mini protease inhibitor mix (Roche). Lysis was carried out by incubation with lysozyme (75 mg/liter of culture) and DNase (100 μg/liter of culture) for 30 min, followed by 12–16 30-s cycles of sonication with 30-s breaks in between. Lysate was cleared by centrifugation and 0.2-μm filtration. Untagged constructs were purified as follows. Ammonium sulfate powder (17.6 g/100 ml) was slowly added to the lysate stirred on ice; precipitates were centrifuged and discarded; then additional ammonium sulfate (12.6 g/100 ml) was slowly added to the supernatant to precipitate the crystallins. The precipitate was collected following centrifugation, resuspended with 8 ml of sample buffer (10 mM ammonium acetate, 50 mM NaCl, pH 7.4) at 18 °C, then cleared by centrifugation and 0.2-μm filtration, and purified by size exclusion chromatography using a Hi-Prep Sephacryl S-100 26/60 column (GE Life Sciences) following the manufacturer's instructions. Samples were stored at 6 °C at concentrations of 2–12 mg/ml (for WT) or 1–4 mg/ml (for W42Q) in sample buffer. 1 mM EDTA was added to stock solutions of the $His_6$-tagged constructs. For experiments requiring higher concentrations, W42Q samples were concentrated the day of the experiment using Vivaspin 20 centrifugal concentrators (Sartorius Stedim). Concentration was determined by $A_{280}$ with extinction coefficients of 41,200 $M^{-1}$ $cm^{-1}$ for WT and 35,710 $M^{-1}$ $cm^{-1}$ for W42Q.

*Size Exclusion chromatography*—The monomeric state of the protein samples was confirmed by size exclusion chromatography at 4 °C using the Superdex 75 10/300 GL high resolution column (GE Life Sciences) equilibrated with sample buffer. Injection volume was 250 μl; flow rate was 1 ml/min.

*Protein Stability*—Stability was measured using guanidinium chloride denaturation in 100 mM sodium phosphate buffer with 1 mM EDTA and 1 mM dithiothreitol. Samples at various concentrations of GdnHCl were incubated for 24 h at 37 °C, and intrinsic fluorescence spectra were measured using a Hitachi F-4500 fluorimeter at 10 μg/ml protein concentration, as described (20). The ratio of fluorescence intensity at 320 and 360 nm was used to measure foldedness and to detect the folding intermediate (33). Thermal melting was measured in the same way, except that the sample remained in its native buffer (10 mM ammonium acetate, 50 mM NaCl), and heating was used in place of denaturant. Sample concentration was 1 μM to minimize aggregation. Rate of heating was ~0.9 °C/min. Data are reported as means ± S.E. of three independent melting curves.

*Protein Aggregation*—Turbidity was monitored using either a UV-visible spectrophotometer (Varian) and a 200-μl quartz cuvette (Starna) in 250 μl of volume or a FluoStar Optima plate reader (BMG) and polypropylene 96-well plates (Greiner) in 200 μl volume. In the former case, no agitation was applied; in the latter, plates were shaken gently for 5 s prior to each 60-s measurement cycle. Polymerization experiments were performed in sample buffer (10 mM ammonium acetate, 50 mM

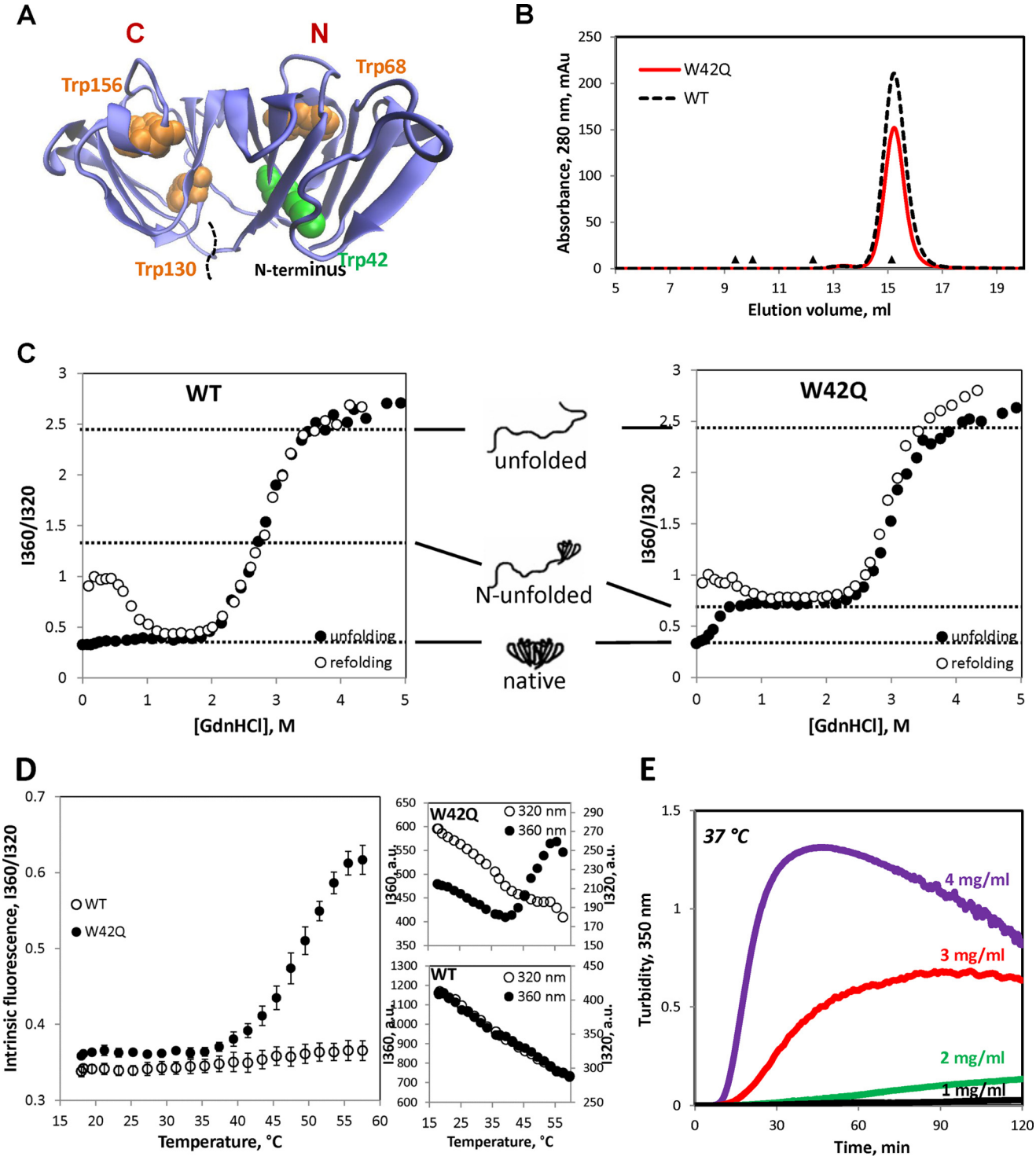


FIGURE 2. *A*, cartoon representation of the HγD crystal structure (24) showing the positions of the four Trp residues. The *dashed black line* indicates domain boundary. Trp-42 is highlighted in green. *B*, W42Q and WT HγD are natively monomeric by size exclusion chromatography. *Black triangles* indicate elution peaks of alcohol dehydrogenase (150 kDa), bovine serum albumin (66 kDa), carbonic anhydrase (29 kDa), and cytochrome *c* (12.4 kDa). Both crystallin constructs are somewhat delayed in their migration relative to their 20-kDa size. The small peaks near 13.5 ml are likely weak dimers: their amplitudes are further reduced in warm samples (data not shown). *C*, equilibrium denaturation curves for untagged WT and W42Q samples at 37 °C. Intrinsic tryptophan fluorescence is used to probe tertiary structure integrity by taking advantage of the anomalously strong intramolecular Trp quenching mechanism in HγD. Ratios of fluorescence intensity at 360 and 320 nm reveal the extent of unfolding at a given concentration of denaturant, guanidinium chloride. The mutant's N-terminal domain unfolds at ~0.3 M GdnHCl, as reported by the red shift in Trp-68 fluorescence. The $I_{360}/I_{320}$ ratio of N-td unfolding is lower for the W42Q mutant than for the WT, because the mutant N-td has one Trp residue *versus* two for the WT. *D*, thermal unfolding of W42Q in the low temperature range without denaturant (means ± S.E. of three replicate melts). Representative curves at right show fluorescence intensities at 360 and 320 nm. *E*, concentration-dependent turbidity development in $His_6$-W42Q solutions at 37 °C without denaturant.

NaCl, 1 mM EDTA, pH 7.4). Maximum growth rate *versus* concentration curves were fitted to two-parameter functions ($y = ax^2 + b$ or $y = ax + b$) using IGOR Pro.

*SDS-PAGE*—Acrylamide gels (14%) were prepared using the Criterion protocol and reagents (Bio-Rad). For pellet-supernatant separations, turbid protein solutions were centrifuged for 10 min at 12,000 × *g* in a tabletop centrifuge, resuspended, and washed with 1 ml of sample buffer three times. Samples were incubated in gel-loading buffer (final concentration 2% SDS, 60 mM Tris, pH 6.8, 6% β-mercaptoethanol) in freshly boiled water for 5 min prior to loading. In the case of TCEP-reduced samples, TCEP concentration was 5 mM. Coomassie-stained gels were digitized using a Typhoon 9400 laser scanner (GE Healthcare).

*Bis-ANS Binding*—Exposure of hydrophobic surfaces was probed using bis-ANS (Sigma-Aldrich) at 10 nM or 1 μM, to which samples from the aggregation time course were added, and fluorescence spectra were measured using a Hitachi F-4500 fluorimeter.

*Thioflavin T Staining*—Amyloid aggregation was induced by shifting the pH of the aggregation reaction from 7 to 3 using acetic acid. Samples from the aggregation time course were mixed (1:200) immediately with a solution of 25 μM ThT in 50 mM sodium phosphate pH 7 buffer. This buffer was used to neutralize the pH of the solution. Fluorescence spectra were measured using a Hitachi F-4500 fluorimeter.

*Filter Trapping*—50-μl samples from aggregating W42Q-only and W42Q+WT (1:4) were centrifuged in 100,000 MWCO regenerated cellulose filters (Millipore). The oligomers and polymers trapped on the filter membrane were washed with 500 μl of sample buffer. The filter membranes were incubated with 50 μl of buffer containing 0.5 mM TCEP, and the resolubilized protein collected in the flow-through was run on 14% polyacrylamide gels alongside dilution series of 10–100 μg/ml of W42Q. Coomassie-stained gels were scanned on a ScanMaker 9800XL optical scanner (Microtek) and quantitated using GelAnalyzer 2010.

*Transmission Electron Microscopy*—Samples from aggregation reactions were diluted to ~0.2 mg/ml final protein concentration, placed on glow-discharged carbon-coated copper-Formvar grids (Ted Pella), incubated at room temperature for 5 min, then blotted with filter paper, and stained for 45 s with 1% uranyl acetate solution. Stained grids were allowed to dry and then imaged using a JEOL-1200 transmission electron microscope.

*Electrospray Ionization Mass Spectrometry*—Stock protein samples were buffer-exchanged into 30% acetonitrile, 0.05% trifluoroacetic acid using C4 spin tips (Protea) and injected directly onto a QSTAR Elite mass spectrometer at 5 μl/min. QSTAR BioTools software was used to deconvolute the *m*/*z* envelopes and extract the molecular weight. To determine whether native state disulfides were present, the stock samples were first incubated with 7.5 mM dithiothreitol at 65 °C for 1 h and then buffer-exchanged and injected onto the ESI instrument as per above. Samples from aggregation reactions were first denatured in 6 M guanidine HCl for at least 1 h at 37 °C in 200 mM ammonium acetate, pH 7, then injected onto a reverse-phase C18 HPLC column, and eluted in a gradient of acetonitrile with 0.05% trifluoroacetic acid. Peak fractions were collected by hand and injected onto the ESI instrument as per above. Instrumental error was 0.001%, or ±0.2 Da.

*Anaerobic Aggregation*—Stock samples were transferred to rubber-stopped glass vials, and the head space was purged on a Schlenk line with argon gas for 10 min. The vials were then sealed, transferred to a custom-designed MBraun anaerobic glove box under nitrogen atmosphere, and allowed to gas exchange for 30 min. Temperature shift and turbidity measurements were carried out using an Agilent 8453 diode array spectrophotometer.

## RESULTS

*The W42Q HγD Mutant Is Stable in the Cold but Aggregates under Physiological Conditions*—The untagged and hexahistidine-tagged HγD W42Q (W42Q and $His_6$-W42Q) expressed in WT-like yield in *E. coli*., were indistinguishable from the wild-type monomer by size exclusion chromatography (Fig. 2*B*), and developed no detectable turbidity for weeks of storage at 4–8 °C at 1–2 mg/ml. Intrinsic fluorescence showed native-like structure at 37 °C but a prominent unfolding intermediate under partially denaturing conditions (Fig. 2*C*), similar to other cataract-linked γ-crystallin core substitutions (8, 21–23). The $I_{360}/I_{320}$ ratio of the N-unfolded intermediate was ~0.7, because the W42Q mutant is missing one of the two Trp residues in the N-terminal domain. The guanidinium unfolding transition midpoint for the W42Q N-td was ~0.3 M.

Because aggregation in our experiments was triggered by a temperature shift rather than chemical denaturation, we determined the temperature range of this first unfolding transition without chemical denaturant. When heated at low concentration (1 μM) in the absence of any denaturant, the midpoint of this unfolding transition for W42Q was ~47 °C; only the very beginning of thermal unfolding fell in the physiological temperature range (Fig. 2*D*). Representative traces of $I_{360}$ and $I_{320}$ intensity (Fig. 2*D*, *right panel*) show a monotonic decline with temperature. This is due to the temperature-dependent decrease in quantum yield of Trp fluorescence (34). No photobleaching of the sample was detectable when the same number of spectra was obtained at constant temperature (data not shown). Nevertheless, at higher concentrations, warming the chilled W42Q sample to 37 °C, at physiological pH and without denaturants, resulted in development of turbidity, indicating aggregation (Fig. 2*E*). Our laboratory has previously reported amyloid aggregates formed by WT γD crystallin at acidic pH (35). The W42Q aggregates reported here, however, did not stain with the amyloid-binding dye thioflavin T or show the distinctive amyloid morphology by negative stain electron microscopy (*data not shown*); they also showed little staining with the hydrophobic exposure probe bis-ANS during the course of aggregation (see Fig. 9*A*). Lack of ThT binding or significant solvent exposure of hydrophobic residues despite steep temperature dependence is consistent with domain-swapped aggregation.

As reported in our previous studies (20, 32, 36, 37), when γ-crystallins are diluted from high to low (<1 M) guanidinium concentrations, aggregation competes with productive refolding. This was observed also for the W42Q mutant (Fig. 2*C*) and

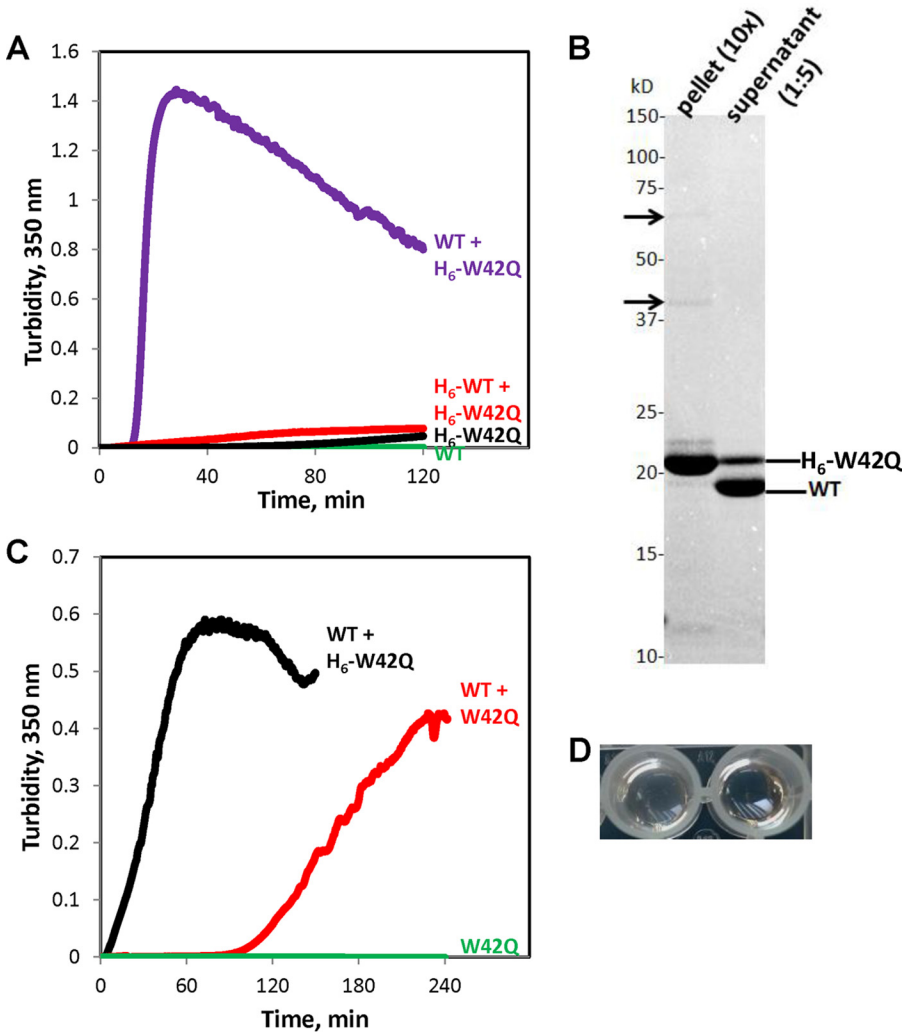


FIGURE 3. **WT/mutant interaction drives aggregation of W42Q HγD.** *A*, turbidity kinetic traces: $His_6$-W42Q at 1 mg/ml with WT or $His_6$-WT at 4 mg/ml. $His_6$-W42Q with filtrate from WT is in *black*. *B*, SDS-PAGE (reducing) of the turbid mixture in *A*. *Arrows* indicate bands consistent with trimers and dimers of W42Q, perhaps because of formation of buried intermolecular disulfides or partially SDS-resistant oligomers. *C*, turbidity traces for tagged (*black*) and untagged (*red*) W42Q at 0.4 mg/ml mixed with untagged WT at 3.6 mg/ml, compared with untagged W42Q at 0.4 mg/ml by itself (*green*). *D*, visible turbidity in 10:1 WT/W42Q mixture (*left*) compared with buffer (*right*) following a 3-h incubation at 37 °C. $H_6$, $His_6$.

precluded measurement of refolding of its N-terminal domain, which would occur in the same range. Thermal denaturation of the C-terminal domain of the mutant or of either domain of the WT protein was measured previously (32) and occurs in a much higher temperature range than what is used here.

*A WT/Mutant Interaction Promotes Aggregation of W42Q HγD*—Oxidation of tryptophan is a relatively rare event (25, 38). Thus, we studied aggregation in WT/W42Q mixtures where most of the protein was WT to test for any prion-like interactions. Such mixtures showed strikingly higher turbidity at 37 °C and pH 7 than the W42Q or WT proteins alone (Fig. 3, *A* and *C*), becoming visibly opaque (Fig. 3*D*).

When a hexahistidine tag is added to the W42Q construct ($His_6$-W42Q), it can be unambiguously resolved from WT by SDS-PAGE. The presence of the tag shortened the apparent lag phase of W42Q aggregation and increased the growth rate relative to that observed for untagged W42Q but did not significantly change the amplitude of turbidity in the WT/W42Q mixtures (Fig. 3*C*). Pellet/supernatant separations of the turbid aggregation mixtures revealed that the aggregated fraction consisted of $His_6$-W42Q alone, whereas the WT protein escaped aggregation and remained in the soluble fraction (Fig. 3*C*). Serendipitously, we found that adding an N-terminal hexahistidine tag to the WT protein almost completely abolished its ability to promote polymerization of the mutant (Fig. 3*A*, *red trace*). Thus, the effect of the WT protein was specific rather than, for example, a molecular crowding effect and could be controlled at the sequence level.

In strongly aggregating mixtures, turbidity declined after an initial rise and plateau (Fig. 3*A*, *purple trace*). This is likely due to both precipitation and gradual condensation of the polymers, because it was also observed in the vertical beam plate reader configuration (Fig. 4, *A*, *C*, and *D*; the declining phases are omitted for clarity).

We checked for the presence of aggregation-inducing ions or small molecule contaminants in the WT sample by filtering the WT stock solution through a 10,000 molecular weight cutoff centrifugal concentrator unit and then incubating $His_6$-W42Q with the flow-through. (The molecular mass of WT HγD is ~20 kDa, so it was not present in significant amounts in the flow-

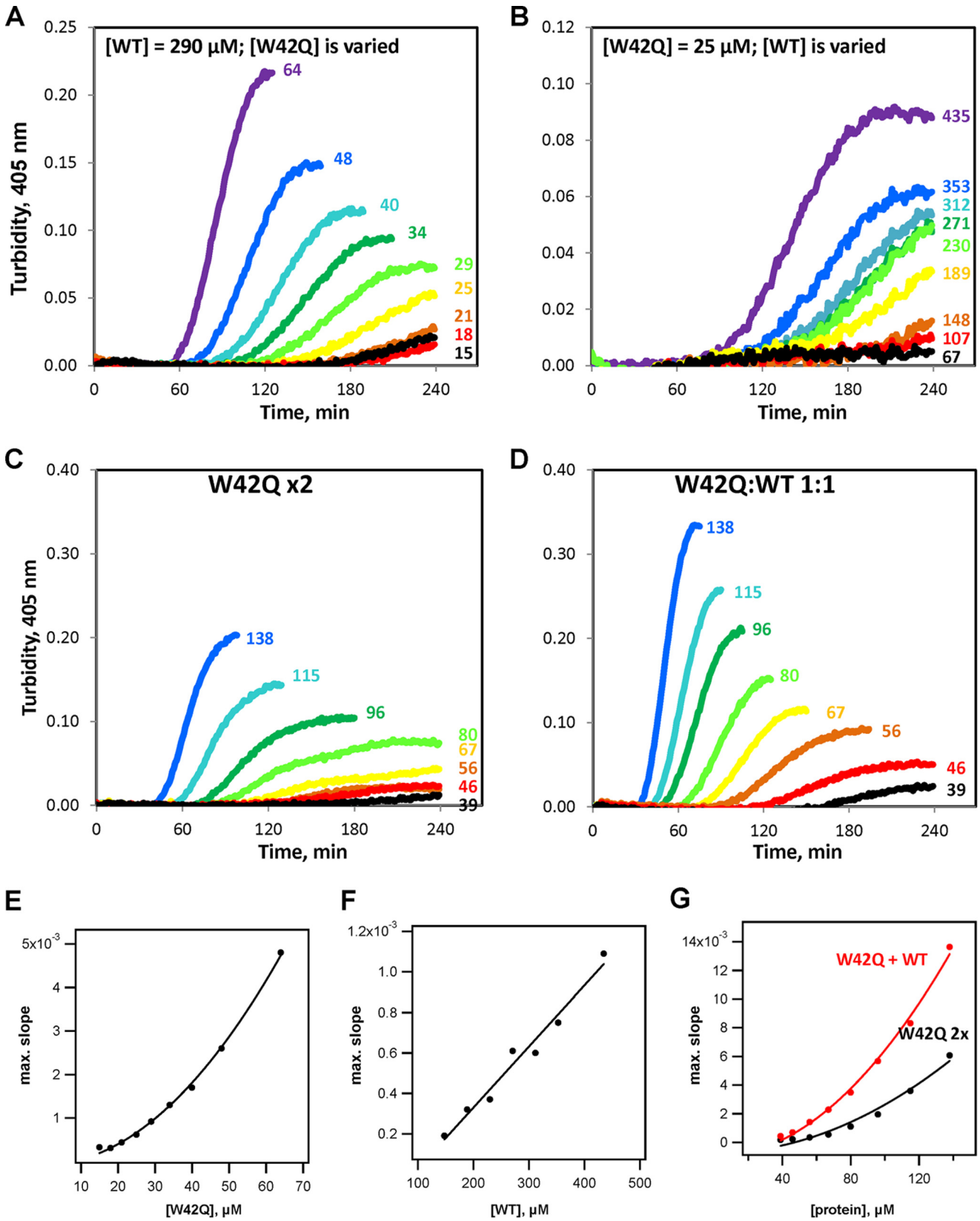


FIGURE 4. **WT has a catalytic effect on W42Q polymerization.** *A–D*, kinetic turbidity traces for variable [W42Q] with constant [WT], with μM W42Q indicated (*A*); variable [WT] with constant [W42Q], with μM WT indicated (*B*); as well as W42Q alone (*C*) and a 1:1 mixture of W42Q and WT at the same total protein concentration (μM, indicated), measured in parallel in 96-well format at 37 °C (*D*). *E–G*, maximum growth rates attained in *A–D* are fitted to quadratic or linear functions. Absolute turbidity values are lower than Figs. 2 and 3 because of the shorter path length in the 96-well format as well as the longer wavelength.

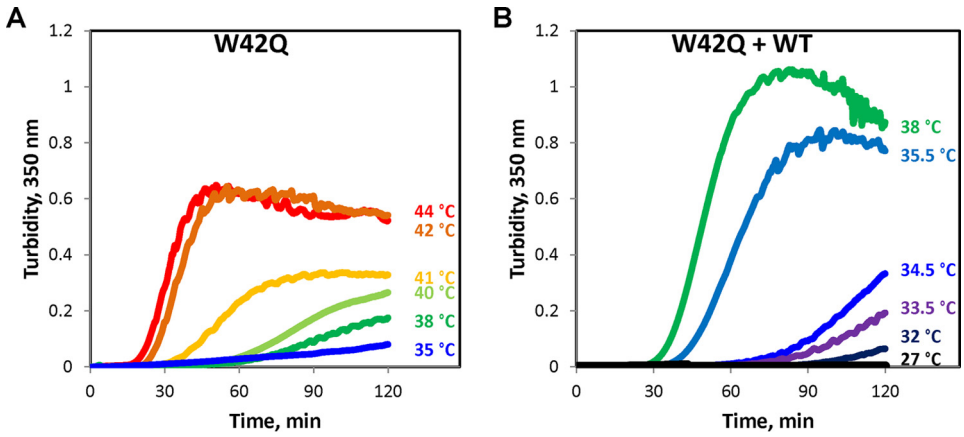


FIGURE 5. **WT downshifts temperature range of W42Q aggregation.** W42Q at 1 mg/ml (*A*) and the WT (4 mg/ml) + W42Q (1 mg/ml) mixture (*B*) both show steep temperature dependence of turbidity development, but in distinct temperature ranges.

through.) The flow-through solution did not promote aggregation of $His_6$-W42Q (Fig. 3*A*, *black trace*).

*WT Has a Catalytic-like Effect on W42Q Polymerization*—Aggregation of W42Q, both by itself and in the presence of a constant amount of WT, followed a quadratic dependence on [W42Q] (Fig. 4, *A*, *D*, and *E*), consistent with nucleation as the rate-limiting step (39, 40). By contrast, when varying concentrations of WT were added to a constant amount of W42Q, the growth rate of the aggregates varied linearly with [WT] (Fig. 4, *B* and *F*). Maximum growth rates were fitted to two-parameter functions (of the form $y = ax^2 + b$ or $y = ax + b$). Because the WT protein is not in the aggregated fraction, its effect has to be viewed as similar to that of a catalyst. Indeed, 1:1 mixtures of WT and W42Q showed shorter lag phase, faster growth rate, and higher amplitude of aggregation than W42Q alone at the same total protein concentration (Fig. 4, *C*, *D*, and *G*). The difference was even more dramatic when $His_6$-W42Q was used (data not shown). Thus, the WT/W42Q interaction is more polymerogenic than the W42Q/W42Q interaction.

Aggregation of W42Q showed steep temperature dependence in the range of 35–42 °C (Fig. 5*A*). The steep temperature dependence of aggregation strongly favors polymerization from a partially unfolded, rather than native, state (41). Notably, this temperature range coincided with the onset of the N-td unfolding transition in the mutant protein (Fig. 2*D*). However, when 4 mg/ml WT was added, the aggregation-permissive temperature range shifted down to 27–36 °C (Fig. 5*B*). Thus, it appears that WT/W42Q binding reduces the temperature needed to allow W42Q polymerization. This is consistent with a catalytic-like effect of the WT protein and suggests that a transient WT/W42Q complex stabilizes the W42Q protein in a partially opened, aggregation-prone conformation.

The presence of the N-terminal $His_6$ tag on the WT protein abolished its catalytic effect (Fig. 3*A*), perhaps by blocking the heterodimerization surface or a subsequent conformational rearrangement. NMR spectroscopy has revealed chemical shifts in a number of residues near Trp-42 and the domain interface with *versus* without the N-terminal His tag (42).

*W42Q Aggregation Depends on Formation of a Non-native Disulfide Bond*—Loss of reducing capacity is a major feature of the aging lens core; oxidative modifications have been found even in normal lenses and more so in cataractous ones (15–17, 43). We compared W42Q aggregation behavior under reducing and nonreducing conditions. Aggregation did not initiate in the presence of strong reducing agents (1 mM DTT or 0.5 mM TCEP), even at 3 mg/ml concentration and 40 °C (*data not shown*). Indeed, adding a reducing agent after turbidity had already begun to develop immediately stopped and then completely reversed the aggregation reaction (Fig. 6*A*).

In advanced nuclear cataract, there is extensive disulfide cross-linking of the crystallin proteins (43), and at least one congenital cataract mutation, R14C, may form intermolecular disulfide cross-links (44). However, the W42Q aggregates contained few intermolecular cross-links. Non-reducing SDS-PAGE of the pelleted aggregate fraction revealed predominantly monomers (Fig. 6*E*), and no higher order oligomers at all were observed by HPLC (Fig. 7). Indeed, the minor dimer, trimer, and higher oligomeric bands seen in Fig. 6*E* may arise during sample preparation, in which the proteins are boiled at relatively high concentration, so thiol/disulfide interchange can occur.

We next tested whether the starting protein samples contained any native state disulfide bonds, whose isomerization might lead to misfolding or cross-linking. Formation of an intramolecular disulfide bond reduces the molecular mass of the protein by 2 Da. However, as shown in Table 1, the molecular masses of all the stock protein solutions obtained by electrospray ionization mass spectrometry matched exactly the theoretical average isotopic molecular masses calculated from the respective sequences and were unchanged under reducing conditions.

The ease with which aggregates were resolubilized by low concentrations of denaturant (Fig. 6*C*) or by a shift to pH 3, which normally stabilizes disulfides (Fig. 6*B*), further supported our conclusion that intermolecular disulfide cross-links are not the cause of W42Q polymerization. Instead, the fact that aggregates dissociated at guanidinium chloride concentrations just sufficient to unfold the native W42Q N-td suggested that a partially misfolded conformation of the N-td required for polymerization may be stabilized by a non-native disulfide bridge.

To search for such an intramolecular disulfide, we turned again to mass spectrometry. Peak fractions from HPLC traces

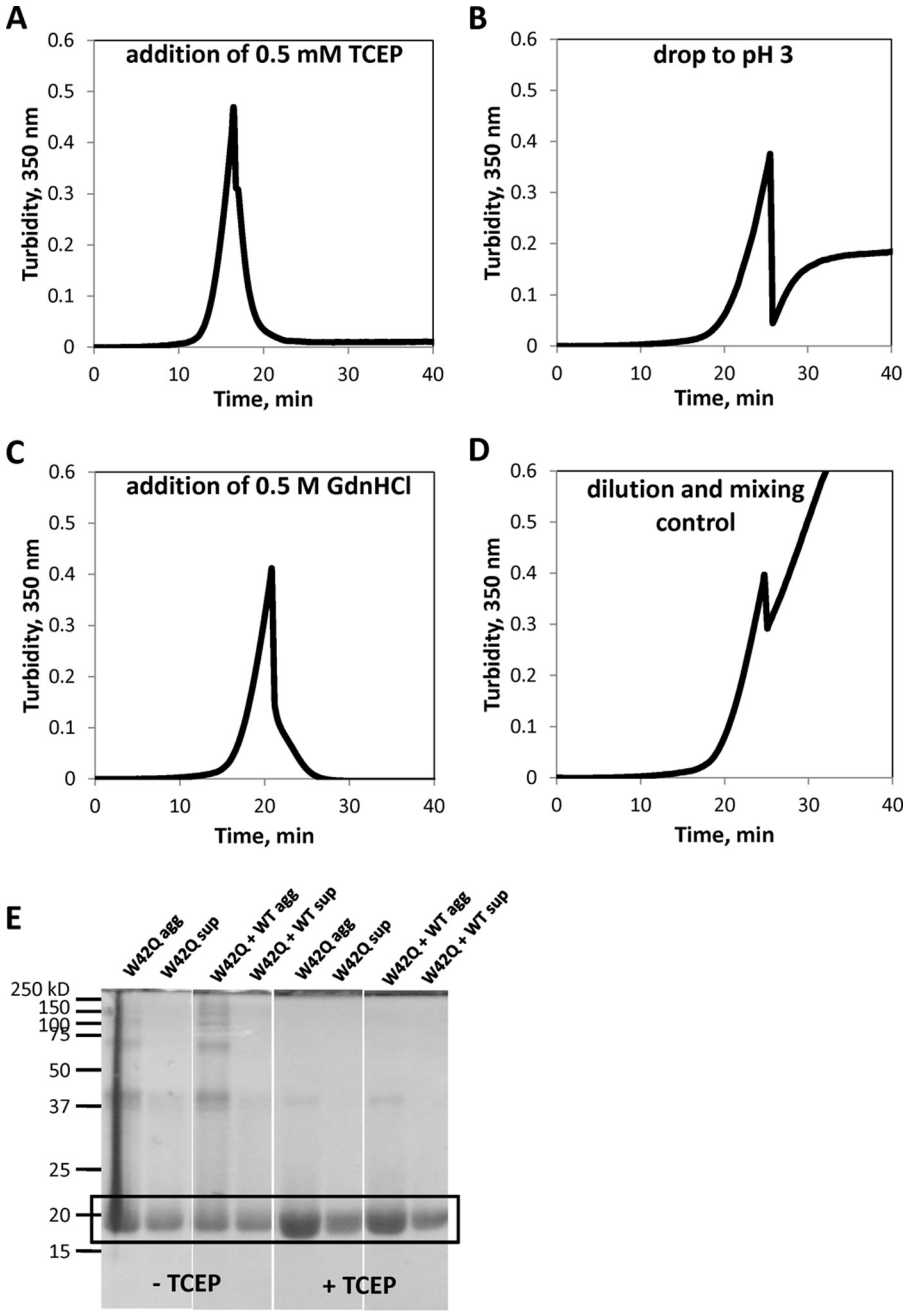


FIGURE 6. **Chemical treatments that solubilize W42Q aggregates.** *A*, addition of the reducing agent tris(2-carboxyethyl) phosphine. *B*, addition of acidic buffer to bring pH down to 3. *C*, addition of guanidinium chloride to a final concentration of 0.5 M, just sufficient to denature the mutant N-terminal domain. *D*, a "mock" control for dilution and pipetting. Aggregation was initiated at 39 °C using 2–3 mg/ml untagged W42Q sample; chemical addition represented a dilution of 10%. *E*, SDS-PAGE of aggregated and supernatant fractions from either W42Q alone (3 mg/ml) or W42Q with WT (1 and 4 mg/ml, respectively) aggregates. Gel samples were prepared in the presence or absence of reducing agent (TCEP). Most of the pelleted protein ran as a monomer in each case; some of the disulfide-bonded dimers and small oligomers likely arose from thiol/disulfide interchange during the sample preparation procedure (boiling in SDS-containing buffer and then 30 min of incubation at 37 °C).

of identically treated soluble and aggregated W42Q fractions from the same temperature shift experiment were analyzed by electrospray ionization (Fig. 7). Although the supernatant fraction showed no detectable disulfide shift, the major peak of the aggregated fraction had a molecular mass 2 Da lower, indicating one disulfide bond per molecule. A minor peak of two-disulfide species was also detectable. We do not yet know which residues are involved in this non-native disulfide, but if a single Cys pair predominates, this observation would open the way to further characterization of both the structural and chemical aspects of the aggregation pathway.

Perhaps because of its low glutathione concentrations, the lens core is maintained at a very low partial pressure of oxygen (45). Our aggregation reactions were carried out under ambient atmosphere. Therefore, protein samples were purged with argon and temperature-shifted under nitrogen atmosphere within an anaerobic glove box. However, there was no detectable difference in turbidity development following this treat-

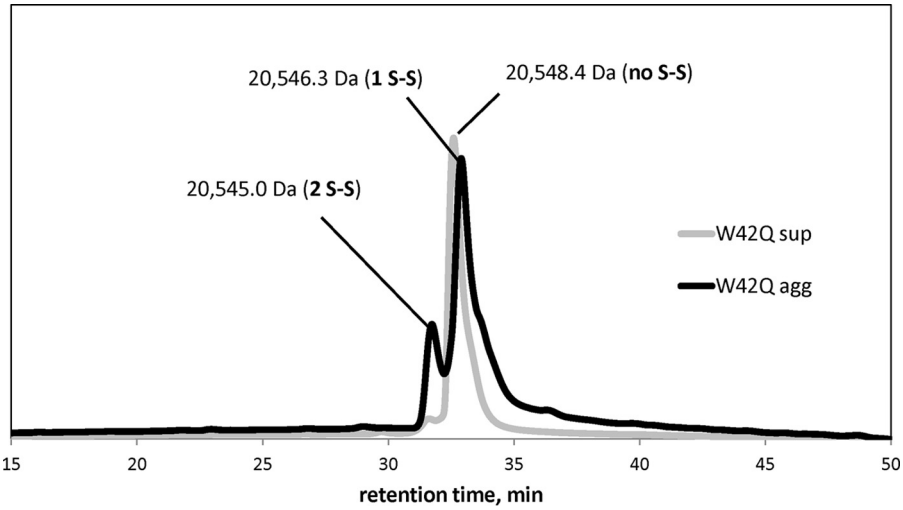


FIGURE 7. **HPLC traces of pelleted *versus* supernatant untagged W42Q protein following 90 min of aggregation at 37 °C at 3 mg/ml.** Soluble and insoluble samples were identically denatured in 6 M guanidinium chloride without reducing agents (this solubilized the pellet), and molecular masses of the indicated HPLC fractions were obtained by electrospray ionization mass spectrometry.

**TABLE 1**

**Predicted and measured molecular masses**

Comparison of molecular masses of the purified WT and W42Q samples predicted from the sequence and obtained by electrospray mass spectrometry in the presence or absence of the reducing agent dithiothreitol. The presence of a native state disulfide bond in the stock sample would reduce the observed molecular mass by 2 Da. The instrumental error is 0.2 Da.

| Stock sample | Predicted molecular mass | Measured molecular mass | |
|---|---|---|---|
| | | No DTT | With DTT |
| | *Da* | *Da* | |
| WT | 20,606.9 | 20,606.6 | 20,606.7 |
| W42Q | 20,548.8 | 20,548.8 | 20,548.9 |

ment compared with temperature shift under ambient atmosphere (*data not shown*). The source of oxidation thus remains unclear, as is the case in the hypoxic eye lens core. Although our samples were purified by size exclusion chromatography, and all aggregation mixtures contained 1 mM EDTA, we cannot rule out trace metal catalysis of disulfide formation.

*Domain Swapping Models of Aggregation*—Molecular dynamics simulations have suggested a swapping pathway via exchange of full globular domains in HγD (46); however, genetic evidence suggests swapping at the N-terminal β-strands instead (14), and such a domain-swap mechanism is consistent with recent force spectroscopy measurements on an HγD polyprotein.[3] That relatively high concentrations of WT are required to promote W42Q aggregation may be due to a relatively weak WT/mutant interaction or to only a small fraction of WT being "active" at any given time.

In Fig. 8, we show two possible models for the observed aggregation behavior. We propose that swapping takes place within the double-Greek key N-terminal domain perturbed by the W42Q substitution and that free W42Q intermediate and W42Q in complex with WT are both polymerogenic. WT increases the total concentration of the mutant in the polymerogenic intermediate conformer and may thereby catalyze the formation of the non-native disulfide, which kinetically traps the mutant in this intermediate state. Two possible modes of action for the WT protein are shown: "nucleation scaffold" and "refolding inhibitor." In the former case, the WT protein acts before the nucleation step of the W42Q polymerization reaction, increasing the number of nuclei; in the latter, WT acts after nucleation, increasing the effective concentration of monomer capable of adding onto pre-existing nuclei. We favor the former model because the apparent lag time shortens with increasing [WT].

A major challenge for the domain-swapping model, recognized early on, is that in the ideal case the aggregates are no more thermodynamically stable than the starting material (47). In this case, either an auxiliary interface is needed or a kinetic trap, as observed in the case of domain-swapped polymers of p13suc1 (48). Although a bound N-terminal $His_6$ tag could provide such an auxiliary interface, in the untagged protein, the non-native disulfide bond is the likely candidate for kinetic trapping.

The detailed mechanism by which the WT protein increases aggregation of the mutant remains to be determined. Linear [WT] dependence (Fig. 4*F*) indicates a catalytic-like process. Weak attractive protein-protein interactions in WT γD crystallin have been inferred from dynamic light scattering (49). Although the aggregates themselves are likely to involve misfolding of the N-td, we note that the C-td of HγD facilitates N-td folding (14). The N-td/C-td interaction contributes ~4.2 kcal/mol to the stability of the N-td in the WT protein (32). Thus, WT HγD at sufficiently high concentration may serve as a source of "decoy" N-tds that would reversibly bind the C-td of W42Q and thus remove this important source of N-td stability (Fig. 8*B*). Whether the WT/W42Q interaction occurs between pats of the N-td or at the N-td/C-td interface, the WT C-td may act as an intramolecular chaperone to rescue the WT N-td from the heteromeric complex.

## DISCUSSION

Turbidity, a simple and sensitive measure of protein aggregation (50), is particularly relevant for cataract disease (20, 23,

[3] S. Garcia-Manyes, personal communication.

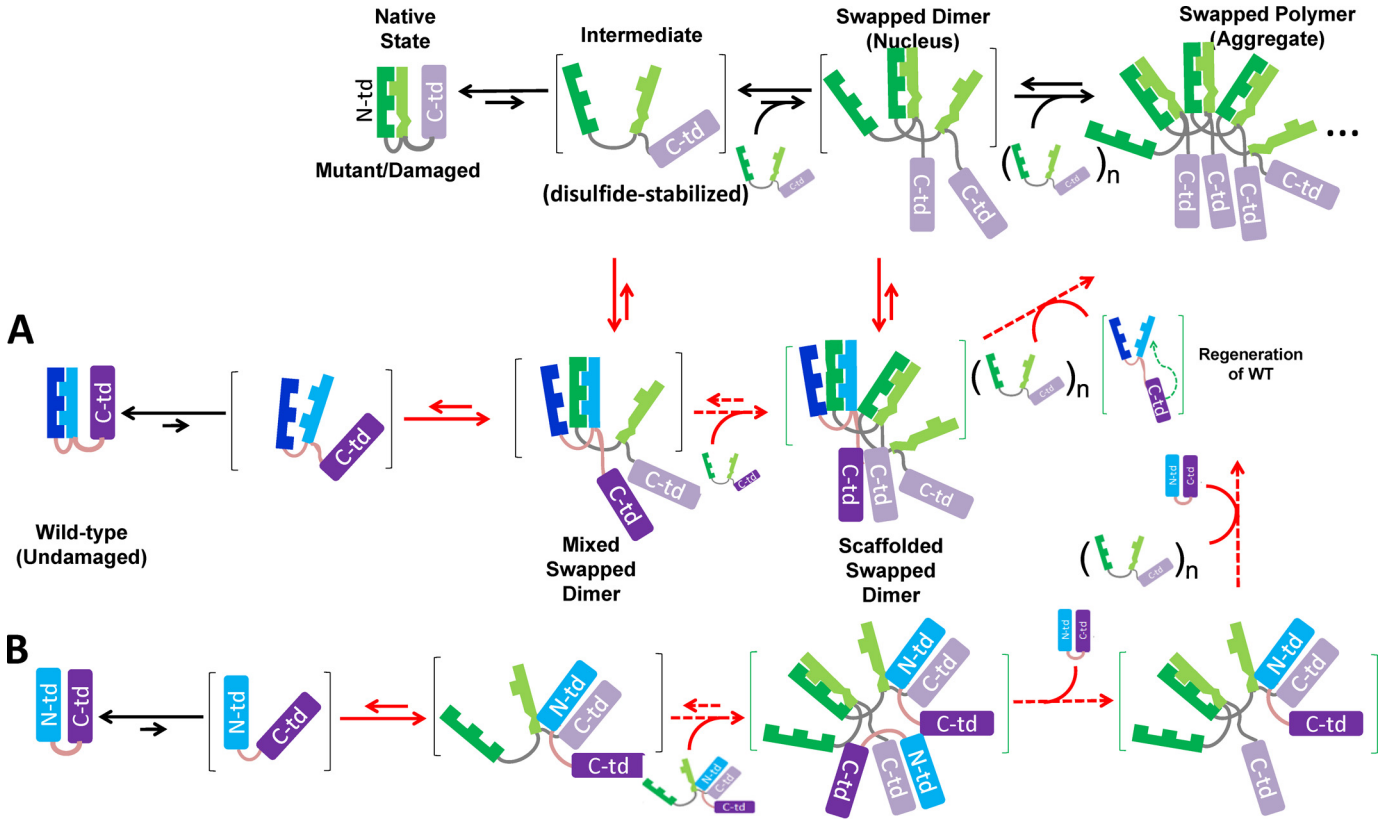


FIGURE 8. **Two possible models of domain-swapped aggregation promoted by WT/mutant domain exchange.** A set of native contacts is weakened in the mutant or damaged N-terminal domain (shown as a missing interaction) and serves as the interface for swapping. The WT intermediate may serve as an inhibitor of W42Q refolding (*solid red arrows*), as a scaffold for nucleation (*dashed red arrows*), or both, depending on when in the assembly pathway it dissociates. The W42Q/WT binding may occur within the N-td (*A*) or at the interface of N- and C-terminal domains (*B*).

27, 51, 52). However, it depends on both size and shape of polymers, thus leaving open the possibility that presence of WT protein shifts the W42Q aggregates into a more extended shape rather than changing the extent of polymerization. Hence, it is valuable to know whether equally turbid solutions of W42Q alone *versus* W42Q + WT contain similar amounts of aggregated material. Fig. 9 shows the empirical relationships between turbidity and bis-ANS staining and turbidity and total polymer concentration (by mass) for W42Q-only and W42Q + WT (1:4) solutions. The relationships are approximately the same for the homogeneous and heterogeneous samples, indicating that greater turbidity in the WT/W42Q mixtures (Figs. 3–5) results from a greater amount of aggregated material relative to W42Q alone. The fact that bis-ANS staining rises only modestly and quickly plateaus is consistent with the hydrophobic exposure probe binding only to oligomeric intermediates or only to aggregate "ends," rather than mature aggregates. A more quantitative treatment of the aggregation process is beyond the scope of the current work.

Mutational effects on protein stability and aggregation are usually studied in homogeneous solutions of the mutant protein, where the effect is assumed to arise directly from the particular mutation. However, where mixed mutant/wild-type solutions have been studied, such as in superoxide dismutase 1, the protein associated with amyotrophic lateral sclerosis, additional interactions emerged. The G85R variant of human superoxide dismutase 1 forms heterodimers with the wild-type protein, leading both to altered enzymatic properties and to possible prion-like conformational conversion (29, 53). Heterodimerization appears to stabilize the mutant protein in a toxic intermediate conformation (53). Notably, overexpression of human wild-type superoxide dismutase 1 accelerates ALS onset in mice carrying the human G85R superoxide dismutase 1 variant, but not the murine G86R variant (54). Other recent examples of destabilizing mutations leading to aberrant WT/mutant interactions and dominant-negative effects include several tumor-associated somatic mutations in p53 (30). We have shown that deleterious WT/mutant interactions are also created by a destabilizing mutation in the core of a human eye lens crystallin. However, this interaction inverts the classical prion-like model: rather than the mutant seeding aggregation of the wild type, it is the wild-type polypeptide that drives aggregation of the mutant in the mixture in a catalytic-like manner. Importantly, WT HγD enables W42Q polymerization even at mutant concentrations or temperatures insufficient for homogeneous nucleation. Similar reactions may underlie polymerization in other proteins following destabilizing chemical modification because of aging or specific environmental exposure.

Only a few types of protein aggregates are currently recognized: amyloid polymers, native state polymers, native state precipitates, cross-linked polymers, nonspecific non-native aggregates, and domain-swapped polymers. ThT-negative, noncovalent, steeply temperature- and concentration-depen-

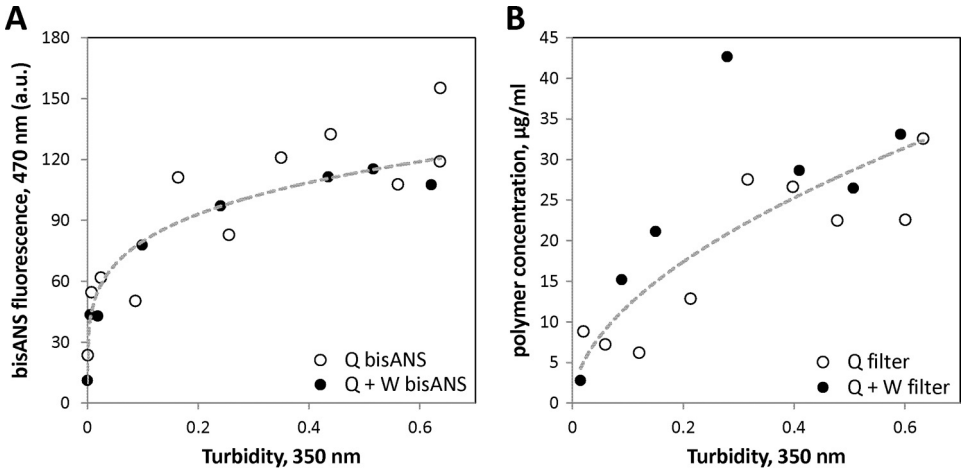


FIGURE 9. **Relationship of turbidity to other measures of protein aggregation.** Bis-ANS fluorescence (*A*) and total polymer mass concentration (*B*) as a function of turbidity are approximately the same for W42Q-only and W42Q+WT (1:4) solutions. The *dashed lines* are empirical, power law fits of the combined data.

dent aggregation without significant increase in hydrophobic exposure and catalyzed by reversible interaction with the corresponding region of the wild-type protein is most consistent with domain swapping mechanisms. Temperature-dependent native state phase separation occurs in concentrated crystallin solutions and has been proposed to underlie some cataracts (51). However, the sign of the temperature dependence is reversed: W42Q aggregates when shifted to warmer temperatures, whereas phase separation is favored in the cold. Wild-type/mutant binding affects the native state polymerization of sickle cell hemoglobin, but the effect is inhibitory (55). In contrast, in HγD it promotes W42Q polymerization.

Domain swapping usually occurs near one of the termini (6). In the native state structure of HγD, the side chain of Trp-42 is hydrogen-bonded to Gly-1 (24). The cataractogenic P23T mutant causes a switch in the hydrogen bond acceptor from Gly-1 to Ser-39 (56), thus potentially unlinking the N terminus from the rest of the core. Crystal structure of the W42R mutant reveals a water molecule within the core between Arg-42 and Ser-39 (8). Reduction in bulk at position 42 following the W42Q mutation likely creates a small cavity, so that Gln-42 and Gly-1 can hydrogen-bond only through water in the native state. Given the observation of water entry in explicit-solvent molecular dynamics simulations (26), we can speculate that an early consequence of WT/W42Q binding is increased water entry into the W42Q N-terminal core. A non-native disulfide bond would then kinetically trap a rearranged conformation of the mutant N-td, exposing the N-terminal β-strands for polymerization.

Domain swapping may reconstitute native-like conformers, as in the case of heat-induced $\alpha_1$-antitrypsin polymerization (57), or alternative conformers, as in the case of its denaturant-induced loop sheet insertion polymerization (58). However, we cannot rule out formation of new compact tertiary structure within the aggregates that differs from any accessible monomeric state. As discussed above, the effect of WT binding may be to stabilize a locally opened W42Q conformer capable of runaway domain swapping.

If the specific WT/W42Q reaction we report occurred *in vivo*, the heterozygote would show more lens turbidity than the homozygous mutant, making W42Q an underdominant allele. Although underdominance is predicted to be a consequence of domain swapping (59), experimental evidence is lacking so far. Collagen has recently been reported to exhibit underdominance for the P549A mutation in the *Y* position of the *G-X-Y* repeat (60). Whether protein aggregation underlies that phenomenon is not yet known. Underdominant alleles are of evolutionary interest because they may cause or maintain species divergence in some cases (61).

It is known that protein sequences can be selected specifically for the ability to suppress homogeneous polymerization of protein folding intermediates (41, 62). A second site mutation (W32S) was recently found that prevents the aberrant heterogeneous WT/mutant interaction in superoxide dismutase 1 (29). Curiously, this single-site difference also controls whether the human and murine variants co-aggregate. We have now found a point mutation that turns the WT HγD crystallin into an aggregation "catalyst" for the mutant and, serendipitously, an N-terminal extension (hexahistidine tag) to the WT sequence that abolishes the enhanced aggregation of the mutant. The W42Q mutation is a mimic of oxidative damage; susceptibility or resistance to other chemical modifications may hinge in part on comparable reactions between native and modified polypeptides. Understanding how a more stable variant in a mixture can specifically drive aggregation of a less stable one has implications for the evolution and design of aggregation-resistant proteins or controllable protein polymers. It can also enable therapeutic interventions aimed at the WT/mutant or unmodified/modified interactions in the heterogeneous protein populations of the aging cell.

*Acknowledgments—We are grateful to R. Schiavoni and R. Cook at the Massachusetts Institute of Technology Biopolymers facility for the mass spectrometry experiments and R. E. Bjork of the Drennan group at Massachusetts Institute of Technology for help with anaerobic experiments. We thank Profs. D. Eisenberg, A. Horwich, K. J. Lampi, L. Quintanar, E. I. Shakhnovich, and C. Slingsby for early feedback on the manuscript; M. Y. Liu and C. Kayatekin for discussion of WT/mutant interactions in collagen and superoxide dismutase 1; O. A. Sergeeva for help with illustrations; and C. Haase-Pettingell for expert technical assistance with protein expression.*

## REFERENCES


1. Horwich, A. (2002) Protein aggregation in disease: a role for folding intermediates forming specific multimeric interactions. *J. Clin. Invest.* **110,** 1221–1232
2. Chiti, F., and Dobson, C. M. (2009) Amyloid formation by globular proteins under native conditions. *Nat. Chem. Biol.* **5,** 15–22
3. Bartels, T., Choi, J. G., and Selkoe, D. J. (2011) α-Synuclein occurs physiologically as a helically folded tetramer that resists aggregation. *Nature* **477,** 107–110
4. Aguzzi, A., and Calella, A. M. (2009) Prions: protein aggregation and infectious diseases. *Physiol. Rev.* **89,** 1105–1152
5. Hartl, F. U., and Hayer-Hartl, M. (2009) Converging concepts of protein folding *in vitro* and *in vivo*. *Nat. Struct. Mol. Biol.* **16,** 574–581
6. Bennett, M. J., Sawaya, M. R., and Eisenberg, D. (2006) Deposition diseases and 3D domain swapping. *Structure* **14,** 811–824
7. Stefani, M., and Dobson, C. M. (2003) Protein aggregation and aggregate toxicity: new insights into protein folding, misfolding diseases and biological evolution. *J. Mol. Med.* **81,** 678–699
8. Ji, F., Jung, J., Koharudin, L. M., and Gronenborn, A. M. (2013) The human W42R γD-crystallin mutant structure provides a link between congenital and age-related cataracts. *J. Biol. Chem.* **288,** 99–109
9. Bosco, D. A., Morfini, G., Karabacak, N. M., Song, Y., Gros-Louis, F., Pasinelli, P., Goolsby, H., Fontaine, B. A., Lemay, N., McKenna-Yasek, D., Frosch, M. P., Agar, J. N., Julien, J. P., Brady, S. T., and Brown, R. H., Jr. (2010) Wild-type and mutant SOD1 share an aberrant conformation and a common pathogenic pathway in ALS. *Nat. Neurosci.* **13,** 1396–1403
10. Shi, Y., Rhodes, N. R., Abdolvahabi, A., Kohn, T., Cook, N. P., Marti, A. A., and Shaw, B. F. (2013) Deamidation of asparagine to aspartate destabilizes Cu,Zn superoxide dismutase, accelerates fibrillization, and mirrors ALS-linked mutations. *J. Am. Chem. Soc.* **135,** 15897–15908
11. Wride, M. A. (2011) Lens fibre cell differentiation and organelle loss: many paths lead to clarity. *Philos. Trans. R. Soc. Lond. B Biol. Sci.* **366,** 1219–1233
12. Moreau, K. L., and King, J. A. (2012) Protein misfolding and aggregation in cataract disease and prospects for prevention. *Trends Mol. Med.* **18,** 273–282
13. Michael, R., and Bron, A. J. (2011) The ageing lens and cataract: a model of normal and pathological ageing. *Philos. Trans. R. Soc. Lond. B Biol. Sci.* **366,** 1278–1292
14. Serebryany, E., and King, J. A. (2014) The βγ-crystallins: Native state stability and pathways to aggregation. *Prog. Biophys. Mol. Biol.* **115,** 32–41
15. Hains, P. G., and Truscott, R. J. (2007) Post-translational modifications in the nuclear region of young, aged, and cataract human lenses. *J. Proteome Res.* **6,** 3935–3943
16. Hains, P. G., and Truscott, R. J. (2008) Proteomic analysis of the oxidation of cysteine residues in human age-related nuclear cataract lenses. *Biochim. Biophys. Acta* **1784,** 1959–1964
17. Wei, M., Xing, K.-Y., Fan, Y.-C., Libondi, T., and Lou, M. F. (2015) Loss of thiol repair systems in human cataractous lenses. *Invest. Ophthalmol. Vis. Sci.* **56,** 598–605
18. Lampi, K. J., Ma, Z., Shih, M., Shearer, T. R., Smith, J. B., Smith, D. L., and David, L. L. (1997) Sequence analysis of βA3, βB3, and βA4 crystallins completes the identification of the major proteins in young human lens. *J. Biol. Chem.* **272,** 2268–2275
19. Keenan, J., Orr, D. F., and Pierscionek, B. K. (2008) Patterns of crystallin distribution in porcine eye lenses. *Mol. Vis.* **14,** 1245–1253
20. Kosinski-Collins, M. S., and King, J. (2003) *In vitro* unfolding, refolding, and polymerization of human γD crystallin, a protein involved in cataract formation. *Protein Sci.* **12,** 480–490
21. Lee, S., Mahler, B., Toward, J., Jones, B., Wyatt, K., Dong, L., Wistow, G., and Wu, Z. (2010) A single destabilizing mutation (F9S) promotes concerted unfolding of an entire globular domain in γS-crystallin. *J. Mol. Biol.* **399,** 320–330
22. Mahler, B., Doddapaneni, K., Kleckner, I., Yuan, C., Wistow, G., and Wu, Z. (2011) Characterization of a transient unfolding intermediate in a core mutant of γS-crystallin. *J. Mol. Biol.* **405,** 840–850
23. Moreau, K. L., and King, J. (2009) Hydrophobic core mutations associated with cataract development in mice destabilize human γD-crystallin. *J. Biol. Chem.* **284,** 33285–33295
24. Basak, A., Bateman, O., Slingsby, C., Pande, A., Asherie, N., Ogun, O., Benedek, G. B., and Pande, J. (2003) High-resolution X-ray crystal structures of human γD crystallin (1.25 angstrom) and the R58H mutant (1.15 angstrom) associated with aculeiform cataract. *J. Mol. Biol.* **328,** 1137–1147
25. Moran, S. D., Zhang, T. O., Decatur, S. M., and Zanni, M. T. (2013) Amyloid fiber formation in human γD-crystallin induced by UV-B photodamage. *Biochemistry* **52,** 6169–6181
26. Xia, Z., Yang, Z. X., Huynh, T., King, J. A., and Zhou, R. H. (2013) UV-radiation induced disruption of dry-cavities in human γD-crystallin results in decreased stability and faster unfolding. *Sci. Rep.* **3,** 1560
27. Wang, B., Yu, C., Xi, Y.-B., Cai, H.-C., Wang, J., Zhou, S., Zhou, S., Wu, Y., Yan, Y.-B., Ma, X., and Xie, L. (2011) A novel cRYGD mutation (p.Trp43Arg) causing autosomal dominant congenital cataract in a chinese family. *Hum. Mutat.* **32,** E1939–E1947
28. Schafheimer, N., and King, J. (2013) Tryptophan cluster protects human D-crystallin from ultraviolet radiation-induced photoaggregation in vitro. *Photochem. Photobiol.* **89,** 1106–1115
29. Grad, L. I., Guest, W. C., Yanai, A., Pokrishevsky, E., O'Neill, M. A., Gibbs, E., Semenchenko, V., Yousefi, M., Wishart, D. S., Plotkin, S. S., and Cashman, N. R. (2011) Intermolecular transmission of superoxide dismutase 1 misfolding in living cells. *Proc. Natl. Acad. Sci. U.S.A.* **108,** 16398–16403
30. Xu, J., Reumers, J., Couceiro, J. R., De Smet, F., Gallardo, R., Rudyak, S., Cornelis, A., Rozenski, J., Zwolinska, A., Marine, J.-C., Lambrechts, D., Suh, Y.-A., Rousseau, F., and Schymkowitz, J. (2011) Gain of function of mutant p53 by coaggregation with multiple tumor suppressors. *Nat. Chem. Biol.* **7,** 285–295
31. Clavaguera, F., Bolmont, T., Crowther, R. A., Abramowski, D., Frank, S., Probst, A., Fraser, G., Stalder, A. K., Beibel, M., Staufenbiel, M., Jucker, M., Goedert, M., and Tolnay, M. (2009) Transmission and spreading of tauopathy in transgenic mouse brain. *Nat. Cell Biol.* **11,** 909–913
32. Mills, I. A., Flaugh, S. L., Kosinski-Collins, M. S., and King, J. A. (2007) Folding and stability of the isolated Greek key domains of the long-lived human lens proteins γD-crystallin and γS-crystallin. *Protein Sci.* **16,** 2427–2444
33. Kosinski-Collins, M. S., Flaugh, S. L., and King, J. (2004) Probing folding and fluorescence quenching in human γD crystallin Greek key domains using triple tryptophan mutant proteins. *Protein Sci.* **13,** 2223–2235
34. Kirby, E. P., and Steiner, R. F. (1970) The influence of solvent and temperature upon the fluorescence of indole derivatives. *J. Phys. Chem.* **74,** 4480–4490
35. Papanikolopoulou, K., Mills-Henry, I., Thol, S. L., Wang, Y., Gross, A. A., Kirschner, D. A., Decatur, S. M., and King, J. (2008) Formation of amyloid fibrils *in vitro* by human γD-crystallin and its isolated domains. *Mol. Vis.* **14,** 81–89
36. Flaugh, S. L., Kosinski-Collins, M. S., and King, J. (2005) Interdomain side-chain interactions in human γD crystallin influencing folding and stability. *Protein Sci.* **14,** 2030–2043
37. Flaugh, S. L., Mills, I. A., and King, J. (2006) Glutamine deamidation destabilizes human γD-crystallin and lowers the kinetic barrier to unfolding. *J. Biol. Chem.* **281,** 30782–30793
38. Chen, J., Callis, P. R., and King, J. (2009) Mechanism of the very efficient quenching of tryptophan fluorescence in human γD- and γS-crystallins: The γ-crystallin fold may have evolved to protect tryptophan residues from ultraviolet photodamage. *Biochemistry* **48,** 3708–3716
39. Ferrone, F. (1999) Analysis of protein aggregation kinetics. *Methods Enzymol.* **309,** 256–274
40. Wetzel, R. (2006) Kinetics and thermodynamics of amyloid fibril assembly. *Acc. Chem. Res.* **39,** 671–679
41. Bershtein, S., Goldin, K., and Tawfik, D. S. (2008) Intense neutral drifts yield robust and evolvable consensus proteins. *J. Mol. Biol.* **379,** 1029–1044
42. Jung, J., Byeon, I.-J., Wang, Y., King, J., and Gronenborn, A. M. (2009) The structure of the cataract-causing P23T mutant of human γD-crystallin exhibits distinctive local conformational and dynamic changes. *Biochemistry* **48,** 2597–2609

43. Truscott, R. J. (2005) Age-related nuclear cataract: oxidation is the key. *Exp. Eye Res.* **80,** 709–725
44. Pande, A., Gillot, D., and Pande, J. (2009) The cataract-associated R14C mutant of human γD-crystallin shows a variety of intermolecular disulfide cross-links: a Raman spectroscopic study. *Biochemistry* **48,** 4937–4945
45. McNulty, R., Wang, H., Mathias, R. T., Ortwerth, B. J., Truscott, R. J., and Bassnett, S. (2004) Regulation of tissue oxygen levels in the mammalian lens. *J. Physiol.* **559,** 883–898
46. Das, P., King, J. A., and Zhou, R. (2011) Aggregation of γ-crystallins associated with human cataracts via domain swapping at the C-terminal beta-strands. *Proc. Natl. Acad. Sci. U.S.A.* **108,** 10514–10519
47. Bennett, M. J., Choe, S., and Eisenberg, D. (1994) Domain swapping: entangling alliances between proteins. *Proc. Natl. Acad. Sci. U.S.A.* **91,** 3127–3131
48. Rousseau, F., Schymkowitz, J. W., Wilkinson, H. R., and Itzhaki, L. S. (2001) Three-dimensional domain swapping in p13suc1 occurs in the unfolded state and is controlled by conserved proline residues. *Proc. Natl. Acad. Sci. U.S.A.* **98,** 5596–5601
49. Wang, Y., Lomakin, A., McManus, J. J., Ogun, O., and Benedek, G. B. (2010) Phase behavior of mixtures of human lens proteins γD and βB1. *Proc. Natl. Acad. Sci. U.S.A.* **107,** 13282–13287
50. Wilcken, R., Wang, G., Boeckler, F. M., and Fersht, A. R. (2012) Kinetic mechanism of p53 oncogenic mutant aggregation and its inhibition. *Proc. Natl. Acad. Sci. U.S.A.* **109,** 13584–13589
51. Siezen, R. J., Fisch, M. R., Slingsby, C., and Benedek, G. B. (1985) Opacification of γ-crystallin solutions from calf lens in relation to cold cataract formation. *Proc. Natl. Acad. Sci. U.S.A.* **82,** 1701–1705
52. Ji, F., Jung, J., and Gronenborn, A. M. (2012) Structural and biochemical characterization of the childhood cataract-associated R76S mutant of human γD-crystallin. *Biochemistry* **51,** 2588–2596
53. Witan, H., Kern, A., Koziollek-Drechsler, I., Wade, R., Behl, C., and Clement, A. M. (2008) Heterodimer formation of wild-type and amyotrophic lateral sclerosis-causing mutant Cu/Zn-superoxide dismutase induces toxicity independent of protein aggregation. *Hum. Mol. Genet.* **17,** 1373–1385
54. Audet, J. N., Gowing, G., and Julien, J. P. (2010) Wild-type human SOD1 overexpression does not accelerate motor neuron disease in mice expressing murine Sod1(G86R). *Neurobiol. Dis.* **40,** 245–250
55. Adachi, K., Ding, M., Surrey, S., Rotter, M., Aprelev, A., Zakharov, M., Weng, W., and Ferrone, F. A. (2006) The Hb A variant (β73 Asp → Leu) disrupts Hb S polymerization by a novel mechanism. *J. Mol. Biol.* **362,** 528–538
56. Ji, F., Koharudin, L. M., Jung, J., and Gronenborn, A. M. (2013) Crystal structure of the cataract-causing P23T D-crystallin mutant. *Proteins* **81,** 1493–1498
57. Yamasaki, M., Sendall, T. J., Pearce, M. C., Whisstock, J. C., and Huntington, J. A. (2011) Molecular basis of $\alpha_1$-antitrypsin deficiency revealed by the structure of a domain-swapped trimer. *EMBO Rep.* **12,** 1011–1017
58. Krishnan, B., and Gierasch, L. M. (2011) Dynamic local unfolding in the serpin α-1 antitrypsin provides a mechanism for loop insertion and polymerization. *Nat. Struct. Mol. Biol.* **18,** 222–226
59. Lynch, M. (2012) The evolution of multimeric protein assemblages. *Mol. Biol. Evol.* **29,** 1353–1366
60. Lindahl, K., Rubin, C.-J., Brändström, H., Karlsson, M. K., Holmberg, A., Ohlsson, C., Mellström, D., Orwoll, E., Mallmin, H., Kindmark, A., and Ljunggren, O. (2009) Heterozygosity for a coding SNP in COL1A2 confers a lower BMD and an increased stroke risk. *Biochem. Biophys. Res. Commun.* **384,** 501–505
61. Nosil, P., and Schluter, D. (2011) The genes underlying the process of speciation. *Trends Ecol. Evol.* **26,** 160–167
62. Mitraki, A., Fane, B., Haase-Pettingell, C., Sturtevant, J., and King, J. (1991) Global suppression of protein folding defects and inclusion body formation. *Science* **253,** 54–58